Tracking Considerations in Selection of Radar Waveform For Range and Range-Rate Measurements

RUIXIN NIU
PETER WILLETT, Senior Member, IEEE
YAAKOV BAR-SHALOM, Fellow, IEEE
University of Connecticut

The conventional approach for tracking system design is to treat the detection and tracking subsystems as completely independent units. However, the two subsystems can be designed jointly to improve system (tracking) performance. It is known that different radar signal waveforms result in very different resolution cell shapes (for example, a rectangle versus an eccentric parallelogram) in the range/range-rate space, and that there are corresponding differences in overall tracking performance. We develop a framework for the analysis of this performance. An imperfect detection process, false alarms, target dynamics, and the matched filter sampling grid are all accounted for, using the Markov chain approach of Li and Bar-Shalom. The role of the grid is stressed, and it is seen that the *measurement-extraction* process from contiguous radar "hits" is very important. A number of conclusions are given, perhaps the most interesting of which is the corroboration in the new measurement space of Fitzgerald's result for delay-only (i.e., range) measurements, that a linear FM upsweep offers very good tracking performance.

Manuscript received October 24, 2000; revised July 5 and November 13, 2001; released for publication November 29, 2001.

IEEE Log No. T-AES/38/2/11436.

Refereeing of this contribution was handled by L. M. Kaplan.

This research was supported by AFOSR under Contract F49620-97-1-0198 and by ONR under Contract N00014-97-1-0502.

Authors' current addresses: R. Niu, Syracuse University, Syracuse, NY; P. Willett and Y. Bar-Shalom, Dept. of Electrical and Computer Engineering, U-2157, University of Connecticut, 260 Glenbrook Rd., Storrs, CT 06269, E-mail: (willett@engr.uconn.edu).

I. INTRODUCTION

The choice of transmitted waveform is an essential concern in radar. The usual approach to system design has been to treat the detection and tracking subsystems as completely separate entities: the two basic functions, automatic detection and tracking, are usually viewed and designed without reference to each other. It is well known, for example, that range and range-rate information from the return of a constant-frequency (CF) transmitted pulse are, respectively, poorer and better than those from a linearly frequency-modulated (LFM) pulse. Consequently, if only range data are observed (the "conventional" case), LFM appears to be preferable. The choice of LFM *up*sweep or *down*sweep seems at this point arbitrary. There has been a great deal of excellent work in signal selection for radar and sonar, with particular attention paid to the coded and frequency-hopped models, and to the resulting ambiguity patterns and measurement-level performance (e.g. [3, 8, 11, 13, 22]). Results such as these are very useful, but in many applications the goal is *system-level* performance, and as will be seen, a good measurement accuracy may not translate to good tracking. As illustrated in Fig. 1, we focus on signal selection to provide good *tracking* performance.

In a classic paper, Fitzgerald [10] noted that for "conventional" radar (meaning no direct observation of range-rate is made) the (time delay) measurements resulting from reception and processing of an LFM waveform are a combination of true range r and range-rate $\dot{r}$:

$$m = r + \dot{r}(f_0 T)/(f_2 - f_1) \tag{1}$$

in which m refers to the range (time delay) corresponding to the measured value of the peak return, f_0 is the center frequency, T is pulse length, and f_1 and f_2 are, respectively, the initial and final values of the swept frequency. Thus the measurements of range are "biased" by the range-rate. The bias is easily modeled, and the author showed that an appropriately modified tracking filter performed very well. It was further noted that there was a significant reduction in tracking error when $f_2 > f_1$. This was explained as being due to the tendency for positive correlation between tracking errors for range and range-rate, which results in a measurement of (1) being "less accurately known" (and hence more informative) when $f_2 > f_1$ than when $f_2 < f_1$.

The work of Fitzgerald is particularly important as it demonstrates the inappropriateness of selection of waveform based on measurement quality alone: the interaction between the measurement and the track can be indirect, but must be accounted for. We assume here that *both range and range-rate are observed*: because the improved range-rate information in CF may offset LFM advantages, the situation is even less

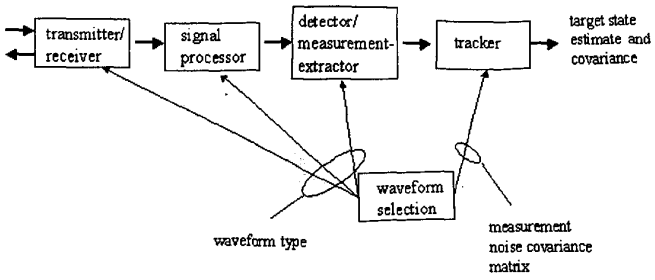

Fig. 1. System block diagram. Waveform is selected and this choice must be shared with all subsystems up to the tracker. Information provided to tracker should be of measurements' locations, and also of their associated covariances, which depend on waveform.

clear. As will be shown, the conclusion of [10] that an LFM-upsweep waveform is best remains usually true.

In [9] the importance of waveform design from a tracking point of view is discussed. The author presents a comprehensive discussion of system considerations for multiple-target tracking, including aspects of both measurement pattern optimization and waveform optimization. Given range-only measurements, direct subtraction of bias as used by Fitzgerald is reasonable, and the tracking performance can be analyzed exactly. With observations of both range and range-rate, analysis becomes complicated, and the inclusion of imperfect measurement association (missed detections and false alarms) makes impossible explicit tracking performance analysis. Some work on the problem includes that of [17], which, building on [16], presents an adaptive waveform selective probabilistic data association (WSPDA) algorithm for tracking a single target in clutter. The assumption of an optimal receiver allows the inclusion of transmitted waveform specification parameters in the tracking subsystem equations, leading to a waveform selection scheme where the next transmitted waveform parameters are selected so as to minimize the average total mean-square tracking error at the next time step. This algorithm does not actually design the optimal waveform; rather, it selects the best waveform from a set of those allowable.

In [26] the relationship between pulse shape and the detection performance was investigated using the algebraic Riccati equation modified by a Markov chain technique (actually a simplified version of hybrid conditional averaging, or HYCA [20]) to account for missed detections but not false alarms. A number of observations were made, among the more important being the confirmation of Fitzgerald's result that for a kinematic target, an *upsweep* LFM signal was superior to *downsweep* LFM and CF pulses. This was seen to arise from the negative correlation between range and range-rate error in the case of an upsweep LFM waveform, and holds particularly for low maneuvering-index targets. There has followed a sequence of papers [6, 23, 24] in which a fuller HYCA routine has been used to account both for missed detections and for false alarms. In parallel to these, [15] has also used the HYCA technique for system-level performance evaluation; that work differs in that (as in [16, 17]) signal selection is dynamic from scan to scan, but there is less consideration of the measurement extraction process.

In [26] resolution cells were defined as the parallelograms that enclosed a given probability of detection (P_d) contour. Using this convention, the results can be skewed by sidelobe pop-ups that distort and possibly enlarge the resolution cell. Here there is a more consistent model of the resolution cell.

The present paper collects the preliminary conclusions from [6, 23, 24] and presents a unified set of results, with particular attention to the resolution, measurement extraction, and also accounting for false alarms; some results and discussion are condensed from [25], but there is considerable extension.
In section II considerable attention is paid to the modeling approach. Specifically, we first make clear the detection model, its relation to the ambiguity function, and the method of measurement extraction assumed. We then discuss in some detail the concept of the resolution cell: from a practical perspective there is of course no such thing, but analysis is greatly eased by its use as a theoretical construct. We then make appropriate modification to the multipulse situation of interest in the radar case, and briefly discuss target dynamics and the HYCA analysis tool that yields the final results.

In Section III we give results on the following issues.

1) Among LFM *up*sweep, *down*sweep, and no sweep (i.e., CF), which is best?

2) Is there a reason to use windowing, or is this taken care of by appropriate measurement extraction?

3) Is performance enhanced by a multipulse waveform?

4) Can performance be enhanced through use of a *mis*matched filter?

5) Is the measurement-extraction process important?

6) Are the conclusions generated using our mode of analysis borne out by simulation?

A great deal of simulation is saved through the use of the HYCA analysis tool; the last point corroborates that HYCA results are reliable. As regards the penultimate point, we consider a measurement-extraction scheme whereby contiguous threshold exceedances are interpolated. Alternative approaches in which the "maximum" threshold exceedance is selected, or in which *all* threshold exceedances are reported to the tracker with reliance on its data association capabilities for interpolation, turn out to be quite inferior.

II. MODELING

A. Measurement Extraction

If the transmitted baseband signal is $s(t)$, the matched filter has an impulse response $h(t) = s^*(-t)$; that is, the impulse response of the matched filter is the conjugate time-reversed baseband signal. With $r_i(t)$ the received waveform and $r(t)$ the baseband representation of $r_i(t)$, the output process of the matched filter becomes

$$x(t) = \int s^*(\lambda - t) r_i(\lambda) e^{-j2\pi f_0 \lambda} d\lambda \equiv \int s^*(\lambda - t) r(\lambda) d\lambda \quad (2)$$

where f_0 is the carrier frequency and $s(t)$ is a replica of the transmitted baseband signal.

Receiver processing is assumed, without loss of generality, to be performed at "baseband"; that is, subsequent to carrier-removal via mixing. The (baseband) received signal is modeled as a return from a Swerling 1 target [18], meaning that

$$r(t) = \left(\sum_i A_i\right) s(t,\tau,f_d)\mathcal{I}(\text{target}) + \nu(t) = As(t-\tau)e^{j2\pi f_d t}\mathcal{I}(\text{target}) + \nu(t) \quad (3)$$

where $s(t,\tau,f_d) = s(t-\tau)e^{j2\pi f_d t}$ is a delayed (τ) and Doppler-shifted (f_d) replica of the emitted baseband complex envelope signal $s(t)$, and $\mathcal{I}(\text{target})$ is a target indicator. The complex numbers A_i represent the amplitude and phase of each of the target reflectors. For a Swerling 1 model, the assumption is that there are many such reflectors, each one with a random amplitude and phase. Hence $A = \sum_i A_i$ approaches a complex Gaussian random variable with zero mean and variance $2\sigma_A^2$. It is assumed that $\nu(t)$ is complex white Gaussian noise independent of A, with zero mean and power spectral density $2N_0$.

If the return signal is expected to be Doppler shifted by a frequency f_g and delayed by a time τ_g (the subscript g denotes "grid"), then the appropriate matched filter output is given by

$$x(\tau_g, f_g) = \int s^*(\lambda - \tau_g) e^{-j2\pi f_g(\lambda - \tau_g)} r(\lambda) d\lambda. \quad (4)$$

The detection test is of the magnitude-square matched filter output

$$|x(\tau_g, f_g)|^2 \underset{\text{decide present}}{\overset{\text{decide absent}}{\lessgtr}} \eta \quad (5)$$

against a threshold η whose value is a function of the desired false alarm rate. This forms the basis of our analysis: compute (5) at an appropriate grid of points in delay/Doppler (or range/range-rate) space, and use any threshold exceedances to estimate a target's state.

Of major interest in the sequel is the "ambiguity function" [18, 26], given by

$$\mathcal{A}(\tau, f) = \frac{1}{\left(\int |s(\lambda)|^2 d\lambda\right)^2} \left| \int s(\lambda) s^*(\lambda - \tau) e^{j2\pi f \lambda} d\lambda \right|^2. \quad (6)$$

The ambiguity function specifies the output of the matched filter in the absence of noise; its shape is related to the implied resolution cell and is strongly dependent on the waveform. The importance of the ambiguity function is that the response of the statistic (5) at grid location (τ_g, f_g) to a target having true delay τ_a and true Doppler shift f_a (the subscript a denotes "actual") is given by

$$|A|^2 \mathcal{A}(\tau_g - \tau_a, f_a - f_g) \quad (7)$$

plus a noise term, where A is the normalized complex return amplitude. For the Swerling 1 target model, the multiplier $|A|^2$ has an exponential distribution; the Swerling 3 model was explored in [6], and there was little new to report, and hence we confine study here to the Swerling 1 situation. Perhaps more important, it is *the same for all* (τ_g, f_g) *pairs*. This means that a strong target return will cause many contiguous (and in the case of an ambiguity function with unfortunate sidelobes, some noncontiguous) matched-filter threshold exceedances; and that a weak target return will cause correspondingly few. This is stated in the following.

ASSUMPTION 1 *Observations are exceedances, according to* (5)*, at a grid of delay/Doppler-shift points* $\{\tau_g, f_g\}$*. If a target with complex return amplitude A is present at delay/Doppler-shift coordinates* $\{\tau_a, f_a\}$*, then threshold exceedances are directly computable from* (7).

ASSUMPTION 2 *When contiguous threshold exceedances occur, it is reasonable to take as the estimated target location either their direct or amplitude-weighted averages.*

Other detection-to-measurement strategies are of course possible.

ASSUMPTION 3 *The actual target location* (τ_a, f_a) *has a uniform distribution within the resolution cell defined by the sampling grid. For a target whose actual location is in a "corner" of the resolution cell, this may imply a high miss probability.*

Some model must be made for the target location, and it is reasonable to assume uniformity. From a notional perspective, we model a target at location (τ_a, f_a) as raising a "tent" of height $|A|^2$ (random and exponentially-distributed, according to the Swerling model) and of shape given by the ambiguity function; the system is aware of this through matched filter samples at the grid $\{(\tau_g, f_g)\}$. The stochastic effects considered are thus due to $|A|^2$ (affecting missed detections and measurement accuracy), due to the uniform density on (τ_a, f_a), and due to thermal noise insofar as it results in false alarms. The effect of thermal noise on measurement accuracy is complicated, as, if oversampling is used, the noise samples are dependent; it seems reasonable to assume that this is an effect of second order in the relatively high signal to noise ratios (SNRs) explored here, and thus we ignore the effect.

One scheme for the extraction of a single measurement (from one or more contiguous threshold exceedances) for delivery to a tracker is as a *direct average* at the grid points (matched-filter samples), meaning that we use

$$\begin{aligned}\hat{r}(\gamma, r_a, v_a) &= \frac{\sum_{r_g, v_g} r_g \mathcal{I}(\gamma \mathcal{A}(\tau_g - \tau_a, f_a - f_g) \geq \eta)}{\sum_{r_g, v_g} \mathcal{I}(\gamma \mathcal{A}(\tau_g - \tau_a, f_a - f_g) \geq \eta)} \\ \hat{v}(\gamma, r_a, v_a) &= \frac{\sum_{r_g, v_g} v_g \mathcal{I}(\gamma \mathcal{A}(\tau_g - \tau_a, f_a - f_g) \geq \eta)}{\sum_{r_g, v_g} \mathcal{I}(\gamma \mathcal{A}(\tau_g - \tau_a, f_a - f_g) \geq \eta)}\end{aligned} \tag{8}$$

for which $\mathcal{I}$ denotes the indicator function, and for which these quantities need not be defined if the denominator sums are zero. This scheme was used in [6, 23, 24]; as seen in this paper, the direct-average scheme of (8) is noticeably inferior to *amplitude-weighted* measurement extraction:

$$\begin{aligned}&\hat{r}(\gamma, r_a, v_a) \\ &\quad = \frac{\sum_{r_g, v_g} r_g \mathcal{A}(\tau_g - \tau_a, f_a - f_g) \mathcal{I}(\gamma \mathcal{A}(\tau_g - \tau_a, f_a - f_g) \geq \eta)}{\sum_{r_g, v_g} \mathcal{A}(\tau_g - \tau_a, f_a - f_g) \mathcal{I}(\gamma \mathcal{A}(\tau_g - \tau_a, f_a - f_g) \geq \eta)} \\ &\hat{v}(\gamma, r_a, v_a) \\ &\quad = \frac{\sum_{r_g, v_g} v_g \mathcal{A}(\tau_g - \tau_a, f_a - f_g) \mathcal{I}(\gamma \mathcal{A}(\tau_g - \tau_a, f_a - f_g) \geq \eta)}{\sum_{r_g, v_g} \mathcal{A}(\tau_g - \tau_a, f_a - f_g) \mathcal{I}(\gamma \mathcal{A}(\tau_g - \tau_a, f_a - f_g) \geq \eta)}.\end{aligned} \tag{9}$$

Whichever is used, the expression for the measurement error covariance given that there is at least one detection is

$$\begin{aligned}\mathbf{R}_m = \frac{1}{1 - P_m} \int_{(\zeta) \in \mathcal{R}} \int_{\gamma} \frac{1}{|\mathcal{R}|} \\ \times \mathbf{e}(\gamma, r_a, v_a) \mathbf{e}(\gamma, r_a, v_a)^T p(\gamma) d\gamma \, dr_a \, dv_a\end{aligned} \tag{10}$$

in which γ refers to the magnitude square of the return, $\mathcal{R}$ is the basic resolution cell having volume $|\mathcal{R}|$, P_m is the overall miss probability and $p(\gamma)$ denotes the probability density function of γ. For the error, one uses

$$\mathbf{e}(\gamma, r_a, v_a) \equiv \begin{cases} \begin{bmatrix} \hat{r}(\gamma, r_a, v_a) - r_a \\ \hat{v}(\gamma, r_a, v_a) - v_a \end{bmatrix} & D(\gamma, r_a, v_a) = 1 \\ \begin{bmatrix} 0 \\ 0 \end{bmatrix} & D(\gamma, r_a, v_a) = 0 \end{cases} \tag{11}$$

in which $D(\gamma, r_a, v_a) = 1$ is the event that at least one detection occurs of a target at location (r_a, v_a) and having magnitude square return γ, meaning that it is computed as

$$D(\gamma, r_a, v_a) = \mathcal{I}\left(\bigcup_{r_g, v_g} \{\gamma \mathcal{A}(\tau_g - \tau_a, f_a - f_g) \geq \eta\} \right). \tag{12}$$

The complementary event $D(\gamma, r_a, v_a) = 0$ refers to a missed detection, and the average value of this is

$$P_m = \int_{(\zeta) \in \mathcal{R}} \int_{\gamma} \frac{1}{|\mathcal{R}|} \mathcal{I}(D(\gamma, r_a, v_a) = 0) p(\gamma) d\gamma \, dr_a \, dv_a \tag{13}$$

which is needed in (10). For a Swerling 1 model we have

$$p(\gamma) = \frac{1}{1 + \text{SNR}} e^{-\gamma/(1+\text{SNR})}. \tag{14}$$

The integration over the resolution cell (i.e., over (r_a, v_a)) in (10) and (13) is performed using evaluation over a dense grid of 400 points uniformly spaced within the resolution cell; the integration over γ is explicit. Note that $\mathbf{R}_m$ is the estimation covariance given that there is at least one detection.

The conversion from delay/Doppler to range/range-rate is well known as $r = (\tau c)/2$ and $v = -(c f_d)/(2 f_0)$, with c the speed of propagation and f_0 the transmitted carrier frequency. The procedure of the extraction of a measurement from a set of threshold-exceedances observed on the range/range-rate sampling grid is illustrated in Fig. 2. Note that for sufficient SNR—meaning that with high probability a target causes several threshold exceedances—the averaging inherent to our measurement-extraction procedure yields sub cell accuracy. This is a form of interpolation, and it is clear that the accuracy increases with SNR, as is consistent with the Cramer-Rao lower bound (CRLB) analysis of [7].

False alarms are due to noise alone and are assumed independent. Because the resolution cells are of constant volume and are assumed to be Poisson distributed, the Poisson parameter (average number of false alarms per unit volume) is $\lambda = P_{\text{fa}} f_0 / c^2$.

B. Resolution Cell

From a practical perspective (5) amounts to a bank of filters matched to Doppler-shifted versions of the

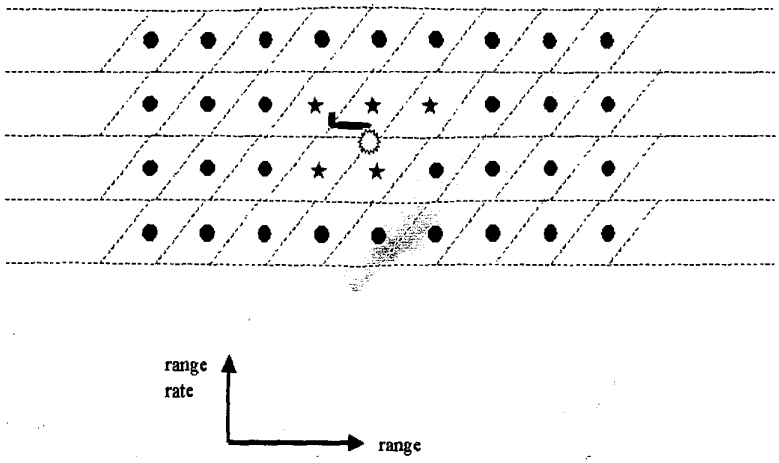

Fig. 2. Illustration of derivation of measurement delivered to tracker. Target's position, denoted by airframe shape, is not at center of resolution cell; resolution cells are parallelograms, and their centers denoted by o's. Threshold exceedances are shown as five-pointed stars, and their average (delivered measurement) as many-pointed star.

transmitted signal separated by Δf Hz, and each of these is sampled every $\Delta\tau$ seconds. The result is a *grid* of matched filter samples $\{\tau_g, f_g\}$, which is most likely rectangular in orientation.

That a target be located at one of these grid samples (i.e., $(\tau_a, f_a) = (\tau_g, f_g)$) would be convenient but is not generally true; thus it is useful to consider a set of delays and Doppler shifts surrounding each sampling point as its *resolution cell.* The term appears to imply that a target within a given resolution cell can yield a detection only at the corresponding center—in a sense that there is a magic "box" in which a target producing a detection must be located—and because of ambiguity function sidelobes and possible oversampling, this is clearly not so. There may also be some implication that all points within the resolution cell are in some sense equivalent, and this also is clearly untrue in that a target actually located between two sampling points (e.g., in a "corner" of the resolution cell) is mismatched to its filter, and has a lower P_d; this, as well as the possibility of detections due to sidelobes, is accounted for here. There is a great deal of confusion about resolution cells.

The rectangular sampling grid is real; the resolution cell is a concept. Nonetheless, the resolution cell is useful both in that it makes statistical averaging over the target's location convenient, and in that it suggests the means by which sampling ought to be configured. With respect to the latter the resolution cell is defined as a tesselating shape (a parallelogram) whose centers form a rectangular grid (the sampling points) and whose orientation and shape are matched to the ambiguity function. Thus, the delay and frequency between sampling points are determined through the ambiguity function by the waveform's duration and bandwidth. As is clear from Fig. 3, the resolution cell $\mathcal{R}$ can be chosen in

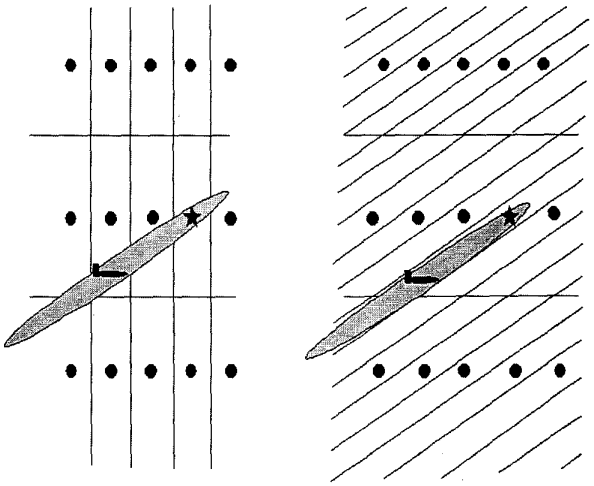

Fig. 3. Possible shape of resolution cells. Bank of matched filters is tuned to evenly spaced Doppler shifts of interest and sampled evenly in time. Result is grid of points in range and range-rate specified by •. Lines indicate boundaries of resolution cells; shaded ellipse is ambiguity function (appearance here is of an ambiguity function for LFM downsweep). On left, rectangular resolution cells: target (location denoted by airframe symbol) causes detection at samples point denoted by star. On right, parallelogram resolution cells.

a number of different ways, but the choice on the right of that figure, where the resolution cell and ambiguity function correspond closely, is more natural for analysis. It seems reasonable to set certain ground rules: 1) the resolution cell pattern forms a tesselating grid, 2) the volume of the resolution cell is fixed, regardless of its actual shape, 3) the resolution cell is oriented and shaped to match, in some sense, the ambiguity function. While consideration 1) could give rise to many different patterns, this section adopts the convention that the resolution cell is a parallelogram. Rule 2) avoids problems of "choppiness" encountered

in [26] and further seems natural from considerations both computational (a constant number of samples per second) and of fairness (all waveforms being examined have the same sampling). Because this measure matches the case of a CF pulse, the constraint that the area of the resolution cell (in (r_a, v_a)-space) must be $(cT) \times (c/(f_0 T)) = c^2/f_0$, in which T is the pulse length is adopted. In the sequel we will explore the effect of the volume of resolution cell (i.e., the sampling effort) on the detection-tracking performance. Thus here is defined a scaling factor $\sqrt{\alpha}$ that controls the resolution cell volume to $\alpha(c^2/f_0)$.

With respect to 3) above it is clear for example that an LFM pulse is ill served by a "rectangular-shaped" resolution cell better suited to CF, and vice versa. To quantify this, the uncertainty in the ambiguity function is measured as

$$\mathbf{R}_{\text{amb}} = \frac{\int_{(r,v)} \begin{pmatrix} r \\ v \end{pmatrix} \begin{pmatrix} r \\ v \end{pmatrix}^T \mathcal{A}(2r/c, -2vf_0/c)\,dr\,dv}{\int_{(r,v)} \mathcal{A}(2r/c, -2vf_0/c)\,dr\,dv} \tag{15}$$

meaning that the ambiguity function $\mathcal{A}$ is treated as a probability density (pdf).

ASSUMPTION 4 *The resolution cell is defined as the parallelogram of a constant volume (area) whose corners satisfy*

$$\begin{pmatrix} r \\ v \end{pmatrix}^T \mathbf{R}_{\text{amb}}^{-1} \begin{pmatrix} r \\ v \end{pmatrix} = \xi \tag{16}$$

and for which ξ is minimized.

This means, from an intuitive perspective, that if the pdf described by $\mathcal{A}$ were Gaussian (it is generally not), the resolution cell as defined would maximize the enclosed probability subject to a volume constraint. The idea is illustrated in Fig. 4. In fact, with reference to that figure and defining

$$\mathbf{R}_{\text{amb}}^{-1} = \begin{pmatrix} \rho_{rr} & \rho_{rv} \\ \rho_{rv} & \rho_{vv} \end{pmatrix} \tag{17}$$

requires simultaneous solution of

$$\begin{aligned} \xi &= \rho_{rr} r_1^2 + 2\rho_{rv} r_1 v_1 + \rho_{vv} v_1^2 \\ \xi &= \rho_{rr} r_2^2 + 2\rho_{rv} r_2 v_1 + \rho_{vv} v_1^2 \\ c^2/f_0 &= 2v_1(r_1 - r_2) \end{aligned} \tag{18}$$

in which r_1, r_2, and v_1 define the resolution cell corners, as shown in Fig. 4. Some algebra results in

$$\begin{aligned} v_1 &= \frac{c}{2\sqrt{f_0}} \left(\frac{\rho_{rr}^2}{\rho_{rr}\rho_{vv} - \rho_{rv}^2} \right)^{1/4} \\ r_1 &= \frac{1}{2} \left(\frac{c^2}{2f_0 v_1} - \frac{2\rho_{rv} v_1}{\rho_{rr}} \right) \\ r_2 &= -\frac{1}{2} \left(\frac{c^2}{2f_0 v_1} + \frac{2\rho_{rv} v_1}{\rho_{rr}} \right) \end{aligned} \tag{19}$$

as the values minimizing ξ.

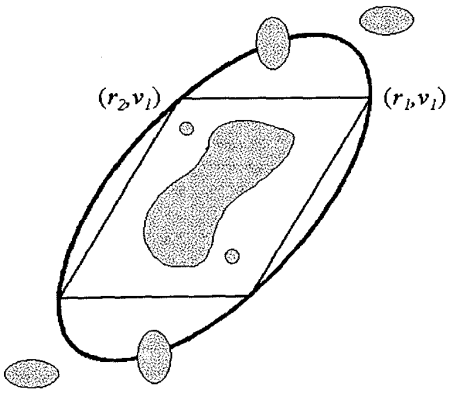

Fig. 4. Illustration of procedure of finding resolution cell. Shaded regions denote range/range-rate values within an ambiguity function contour, meaning that a return with a certain SNR will produce a detection at matched-filter samples within shaded regions. From this, ambiguity function uncertainty $\mathbf{R}_{\text{amb}}$ is formed according to (15) and pictured as ellipse. Actual resolution cell is drawn within that ellipse, according to Assumption 4.

ASSUMPTION 5 *The probability of false alarm is $P_{\text{fa}} = e^{-\eta}$. The probability of a target located at (τ_a, f_a) being missed is $1 - e^{-\eta/(1+\text{SNR}\,\mathcal{A}(\tau_g - \tau_a, f_a - f_g))}$ for the Swerling 1 case.*

The false alarm and miss probability expressions are reasonably well known and are justified in [26]. The miss probability is for a target located at (τ_a, f_a) within the resolution cell with sampling point (τ_g, f_g): because of the model if at least one detection is due to the target, a threshold exceedance must be recorded at that point. The overall miss probability is again computed using the average over all (uniformly distributed) $(r_a, v_a) \in \mathcal{R}$.

It is worth mentioning that in [6] the orientation of the resolution cell was explored. From a geometric perspective, the parallelogram can be oriented to have either vertical or horizontal sides. This consideration has no effect on volume (i.e., the sampling effort), but a considerable effect on the relative density of matched-filter samples taken in range versus range-rate, as is illustrated in Fig. 5. The surprising conclusion from [6] was that the orientation has essentially no effect at all: the accuracy of an extracted measurement stems from the interpolation between threshold exceedances, and not from the exact pattern.

C. Multipulse Operation

The mode of analysis just presented formed the basis for [6], and in that paper results were presented for a parameter set most representative of the *sonar* situation. A major difference between the radar and sonar cases is such that in the former it is unlikely that a reasonable radar target could emerge from the zero-Doppler resolution cell, and

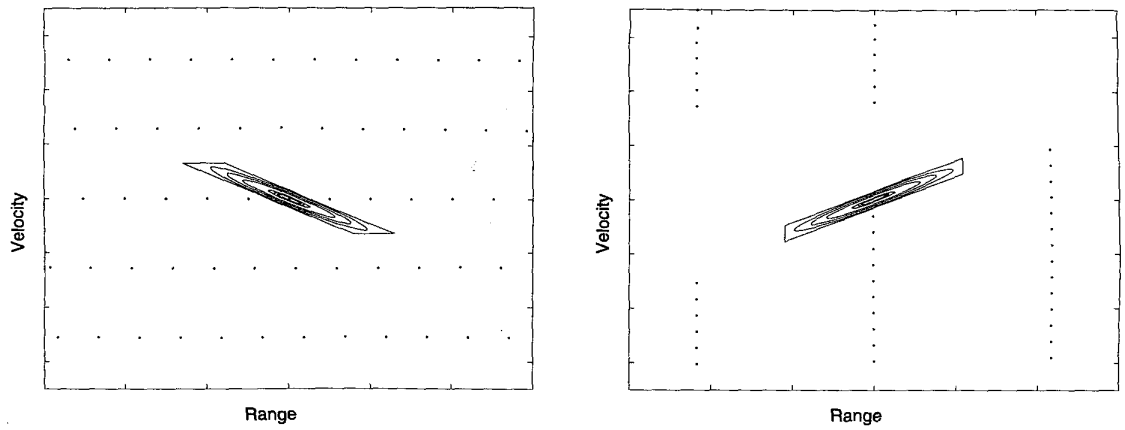

Fig. 5. Sampling patterns with same sampling effort. Left: LFM upsweep resolution cell is shown dense in range and sparse in range-rate. Right: LFM downsweep resolution cell sparse in range and dense in range-rate. In addition to its illustration of complementary sampling patterns, this figure illustrates difference in range/velocity correlation of measurement errors between LFM upsweep and downsweep.

hence the assumptions of the previous analysis would be untenable. References [7, 9] show that in many systems only the zero-Doppler matched-filter output is interrogated, and in the case of LFM this means that the resulting range and range-rate correlation can and should be incorporated, as discussed in [5, 10]. One way to "escape" the zero-Doppler resolution cell is to allow for coherent multipulse operation.

The ambiguity function of a pulse train is now of interest. If the envelope of each pulse of unit energy is $s_n(t)$, then that of a train of N_p equally spaced and coherent pulses is

$$s(t) = \frac{1}{\sqrt{N_p}} \sum_{n=0}^{N_p-1} s_n(t - nT_R) \tag{20}$$

where T_R is the pulse-repetition period. In some implementations, a "staggered" pulse-repetition time [27] is used to avoid ambiguity; that is not explored here. The division by $\sqrt{N_p}$ will maintain unit energy for the entire train. For a uniform (i.e., constant frequency) pulse train $s_n(t)$ is

$$s_n(t) = \begin{cases} 1, & 0 \le t < t_p \\ 0, & \text{elsewhere} \end{cases} \tag{21}$$

where t_p is the pulse length. For an LFM pulse train, $s_n(t)$ is

$$s_n(t) = \begin{cases} e^{jb(t+nT_R)^2}, & 0 \le t < t_p \\ 0, & \text{elsewhere} \end{cases}. \tag{22}$$

The parameter b controls the LFM sweep rate, the total frequency sweep being $b(t_p + (N_p - 1)T_R)/\pi$ Hz.

An ambiguity function for an LFM pulse train is shown in Fig. 6. Such an ambiguity function consists of many replicas, and sometimes it is referred to as a "bed of nails." According to the techniques of [24], all threshold exceedances from all replicas would be averaged to obtain a measurement. This is not realistic. The posterior uncertainty from tracking can restrict attention to only one (primary) ambiguity function replica, and if this is not the case it is argued that the target track is so inaccurate that it can be considered lost. At any rate, from [18], the spacing between replica peaks is T_R in delay and $1/T_R$ in Doppler. Thus, as the "neighborhood," the rectangles in Fig. 6 are assumed, and Assumption 6 below replaces Assumption 1. The borders along the delay and Doppler axes are $[-T_R/2 \quad T_R/2]$ and $[-1/2T_R \quad 1/2T_R]$, respectively.

ASSUMPTION 6 *Observations are exceedances by* $\{|x(\tau_g, f_g)|^2\}$ *of a threshold* η *within the rectangular neighborhood of dimension* $T_R \times 1/T_R$ *around the main peak, according to* (5)*, at a grid of delay/Doppler-shift points* $\{\tau_g, f_g\}$*. If a target with complex return amplitude* A *is present at* $\{\tau_a, f_a\}$*, then threshold exceedances are directly computable from* (7).

Because of this, the area of the basic resolution cell (in (r_a, v_a)-space) is chosen as $(ct_p) \times (c/f_0 N_p T_R) = c^2 t_p / f_0 N_p T_R$. When a scaling factor $\sqrt{\alpha}$ controls the sampling effort, the resolution cell volume becomes $\alpha(c^2 t_p / f_0 N_p T_R)$. Note that the parameter α controls the number of samples per unit volume in range $\times$ range-rate: the sampling *pattern* remains a function of the resolution cell orientation, in that a higher bandwidth waveform (e.g., LFM) confers denser sampling in range and less dense in range-rate. Here false alarms have Poisson parameter[1] (average number of false alarms per unit volume) $\lambda = P_{\text{fa}} f_0 N_p T_R / \alpha c^2 t_p$.

[1]The number of false alarms has actually a binomial distribution for which the Poisson distribution is a good approximation.

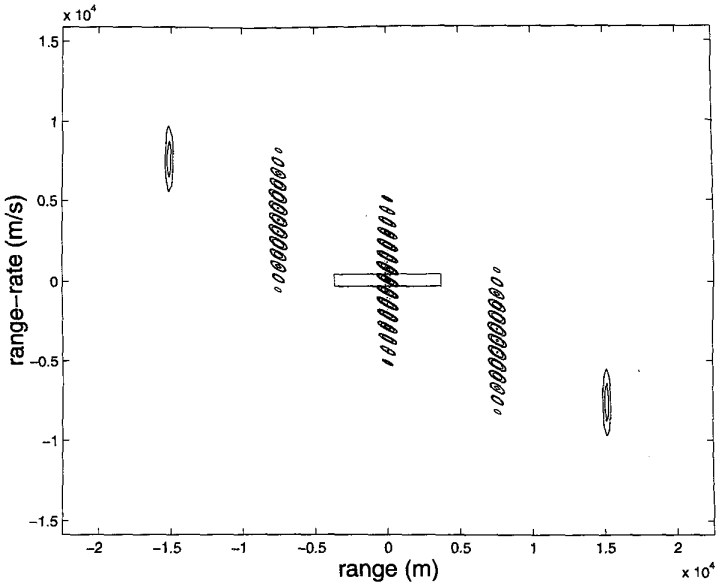

Fig. 6. Ambiguity function contours and neighborhood region around main peak for LFM pulse train, $t_p = 10$ μs, $T_R = 50$ μs, $N_p = 3$, sweep rate of 2 GHz/s. In this notional figure, number of pulses $N_p = 3$ here is lower (and hence so is overall effective total frequency sweep) than in most practical applications, the better to illustrate ambiguity function appearance. For more realistic numbers refer to Figs. 9 and 12.

D. Target Motion and State Estimation

We use the usual kinematic model (e.g. [1]) for target motion

$$\mathbf{x}(k+1) = \mathbf{F}\mathbf{x}(k) + \mathbf{v}(k) \tag{23}$$

where the process noise is white with covariance $E\{\mathbf{v}(k)\mathbf{v}^{\mathbf{T}}(k)\} = \mathbf{Q}(k)$ and zero-mean. In most conventional LFM systems direct observations are of delay, meaning range alone. In contrast, the observations here are delay and Doppler-shift

$$\mathbf{y}(k) = \mathbf{H}\mathbf{x}(k) + \mathbf{w}(k) \tag{24}$$

where the measurement covariance $E\{\mathbf{w}(k)(\mathbf{w}(k))^T\} = \mathbf{R}$ is a function of the waveform shape employed. Thus we have

$$\mathbf{F} = \begin{bmatrix} 1 & \Delta t \\ 0 & 1 \end{bmatrix}$$
$$\mathbf{H} = \begin{bmatrix} 2/c & 0 \\ 0 & -2f_0/c \end{bmatrix} \tag{25}$$
$$\mathbf{Q} = \sigma_v^2 \begin{bmatrix} \frac{\Delta t^4}{4} & \frac{\Delta t^3}{2} \\ \frac{\Delta t^3}{2} & \Delta t^2 \end{bmatrix}$$

where Δt represents the time between measurements (i.e., matched-filter samples), c is the propagation speed in the medium, f_0 is the carrier frequency, and σ_v^2 is the variance of the piecewise constant white process noise (25) [1]. That is, the target model is kinematic with range and range-rate as state variables. For clarity we work in one dimension—range—because it is in this domain that the differences between the various waveform types become apparent; σ_v should be the order of the rms target acceleration [1].

E. HYCA Analysis Model

The system under consideration has elements of detection, measurement extraction from detections, and tracking based on these measurements. Given such interplay, and faced with performance evaluation, a Monte Carlo analysis is tempting; but conclusions drawn from purely simulational evidence are often both unsettling and unsatisfying, and in any case since many factors are being considered and varied the number of Monte Carlo runs would be huge. Thus, an alternative tack using purely analytical techniques would be appealing. For example, CRLBs of delay and Doppler shift have been derived for many transmitted waveforms (e.g. [7]), and it is straightforward to insert these into a Kalman filter, with a final result from interrogation of its steady state. Unfortunately analytical tools like these rely on fairly strict assumptions, these including that the measurement extraction be a perfect maximum-likelihood estimate, that ambiguity-function sidelobes do not confuse the issue,[2] and that there is

[2]Realistically, some locations of the target relative to the sampling grid do not yield detections, and some do. Among those that do, some have associated larger variances than others. Equations (8)–(13) capture best these peculiarities.

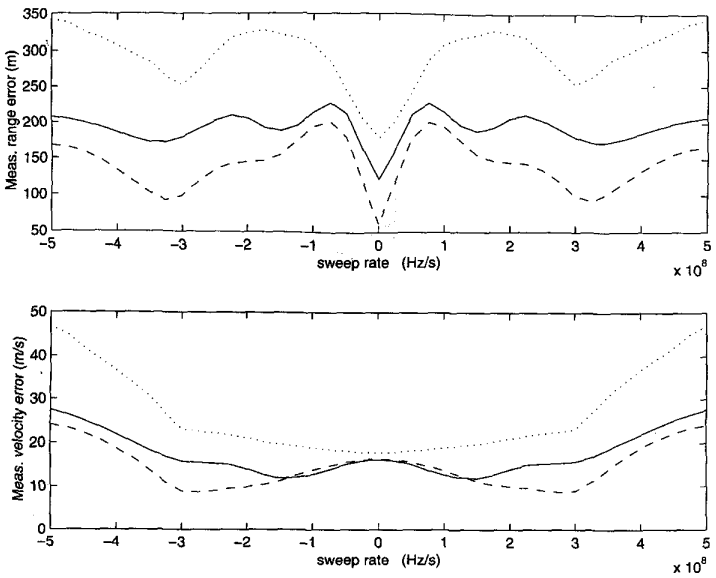

Fig. 7. Measurement range and range-rate error as functions of sweep rate for LFM pulse train, $\alpha = 0.17$, $N_p = 20$. Measurement extraction schemes are strongest return (dotted), direct-average (solid), amplitude-weighted (dashed).

no uncertainty as to measurement origin (false alarms and missed detections).

Reference [20] provides the HYCA (hybrid conditional averaging) procedure of performance evaluation. The tool is analytical and restrictive assumptions are unnecessary. The key is in the use of an underlying and hidden Markov chain, in which the "states" refer to the number of *validated* measurements [2] at each scan. It is assumed that the underlying tracker is a probabilistic data association filter (PDAF). We are merely users of HYCA, and do not discuss it here.

III. RESULTS

Unless otherwise specified, we use in the following

$P_{\text{fa}} = 10^{-3}$,
$\Delta t = 1$ s,
speed of propagation $c = 3 \times 10^8$ m/s,
carrier frequency $f_0 = 4$ GHz,
pulse length $t_p = 10$ μs,
pulse repetition period $T_R = 50$ μs,
$N_p = 20$ pulses,
SNR = 20 dB.

The SNR is in the "aggregate" sense, meaning that coherent integration of all pulses yields performance corresponding to that metric.

Intuition is often guided by the concept of *maneuvering index* [1], defined as

$$\lambda_{\text{man}} = \sigma_v(\Delta t)^2/\sigma_w \tag{26}$$

a parameter proportional, in some sense, to a target's elusiveness to tracking. The denominator is the standard deviation of the measurement noise, which we take as $\sigma_w = cT/2\sqrt{12} = 433$ m. The numerator parameter σ_v^2 (the process noise variance) is usually taken as one of 10, 100, 1,000, or 10,000. with corresponding maneuvering indices $\lambda_{\text{man}} = 0.008$, 0.02, 0.07, and 0.2. In the figures which follow, distance units are in meters and velocity in meters per second. The analytically expressible ambiguity functions are taken from [7]. Other ambiguity functions are integrated via fast Fourier transform (FFT) with adaptive step size.

A. LFM Multipulse Waveforms

1) *Sweep Rate*: Results for an LFM pulse train are shown in Figs. 7–9. In these plots the effects of several different measurement extraction schemes are shown, and these are discussed shortly; for the present discussion note that trends are the same for each. At any rate, in terms of *measurement* quality (Fig. 7) there is no difference between *down*sweep and *up*sweep. First, observe that because the resolution cell experiences a marked change in orientation (it becomes an eccentric parallelogram) as the sweep rate increases, the sampling grid of v_g decreases its fineness as absolute sweep rate increases, and there is a corresponding decrease in velocity *measurement* accuracy.

Next, note that sweep rate has little effect on the *measurement* range error. This may appear surprising. As was stated earlier, and may be found in [7], LFM waveforms are generally known to have better resolution in range than do CF waveforms. In fact, the range error is comparatively low only if the range-rate is already known fairly accurately from

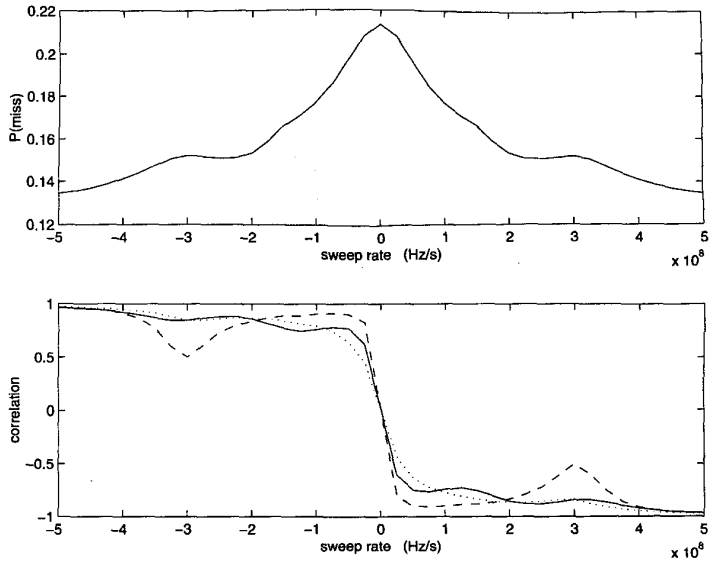

Fig. 8. Probability of miss and correlation coefficient as functions of sweep rate for LFM pulse train, $\alpha = 0.17$, $N_p = 20$. Measurement extraction schemes are strongest-return (dotted), direct-average (solid), amplitude-weighted (dashed).

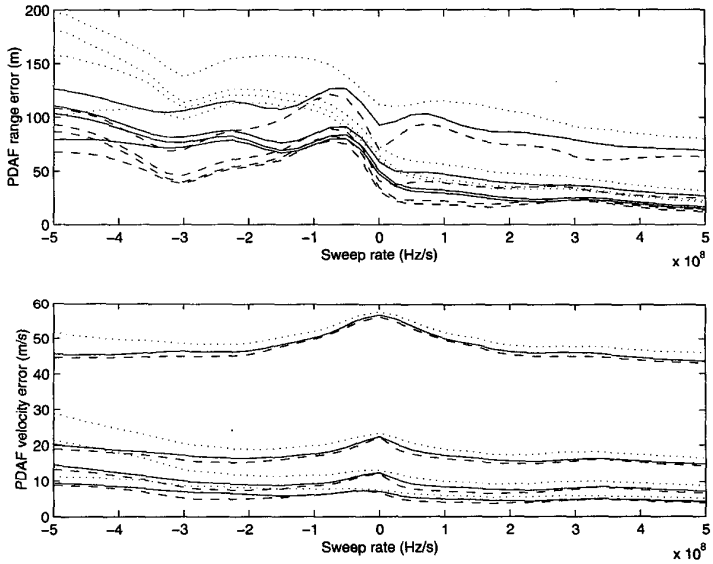

Fig. 9. Estimation range and range-rate error as functions of sweep rate for LFM pulse train, $\alpha = 0.17$, $N_p = 20$, $t_p = 10$ μs, $T_R = 50$ μs. In each figure, bottom, middle, and top curves refer to $\sigma_v^2 = 10$, 100, 1,000, 10,000. Measurement extraction schemes are strongest return (dotted), direct-average (solid), amplitude-weighted (dashed).

previous tracking information. If there is no prior information about a target's range-rate at all, then an LFM waveform is intrinsically no better than CF at measuring range.[3]

Finally and probably of greatest importance: as is clear from Fig. 8, the correlation[4] between range and range-rate measurements is positive in the former and negative in the latter. *The dependable superiority, in terms of range estimation, of LFM upsweep as opposed to LFM downsweep or CF and as previously noted in* [9, 10, 26] *and elsewhere, is clear from Fig.* 9. The reason is, of course, that the estimation error for a

[3]It is important to realize, however, that prior information need not come from tracking. For example, the parameters may be such that a target is constrained to have range rate deep within the zero-Doppler resolution cell. In such cases the assumption of uniformity within the resolution cell is untenable, and although we expect the conclusions to be similar, a different mode of analysis would be necessary.

[4]For a 2×2 covariance matrix $\mathbf{A}$, the correlation coefficient is $A_{1,2}/\sqrt{A_{1,1} \times A_{2,2}}$.

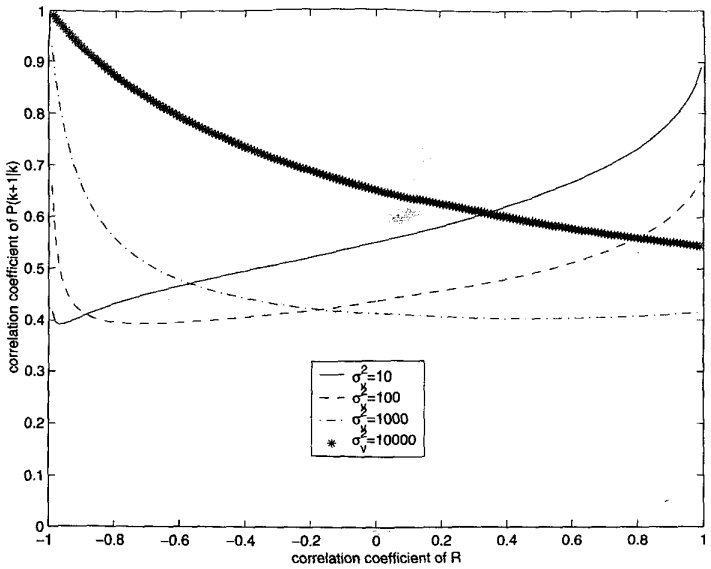

Fig. 10. Steady-state correlation coefficient between range and range-rate prediction errors (i.e., $\mathbf{P}(k+1 \mid k)$) computed via the algebraic Riccati equation, and plotted as function of correlation coefficient between range and range-rate measurements. Parameters used are $\Delta t = 1$ s, and range and range-rate measurement error standard deviations 200 m and 20 m/s, respectively, taken as typical from Fig. 7.

kinematic target tends to exhibit positive correlation between position and velocity. This is explored quantitatively in Fig. 10, in which the correlation coefficient between range and range-rate *prediction errors* (i.e., $\mathbf{P}(k+1 \mid k)$) is plotted as a function of that of the *measurement errors* (i.e., $\mathbf{R}$). Fig. 10 is a steady-state result, and is obtained from the algebraic Riccati equation. The main message from Fig. 10 is that range and range-rate estimation errors are indeed positively correlated regardless of whether or not the measurement errors are; thus, if the currently predicted track is treated as *prior* information, then overall accuracy is enhanced by a measurement having complementary characteristics, meaning an LFM upsweep with its *negatively* correlated position and velocity measurements.

It is also clear from Fig. 9 that the sensitivity to the choice of waveform *decreases* as the target becomes more agile (higher σ_v). As to the latter observation, consider that a larger σ_v corresponds to prior information of lower quality (higher motion uncertainty). With poorer prior localization the tracking system is forced to rely more heavily on each measurement as it becomes available, and this is illustrated in Fig. 11.

As is explored quantitatively in Fig. 12, in which the optimal sweep rate is determined as a function of maneuvering index, the best sweep rate decreases as the maneuvering index increases. This is an indication that for low-maneuvering targets the orientation of the prior (tracking error) covariance ellipse becomes more horizontal ([2, p. 452]), as shown in Fig. 13. A higher sweep rate confers greater posterior accuracy on position measurements, and less on velocity

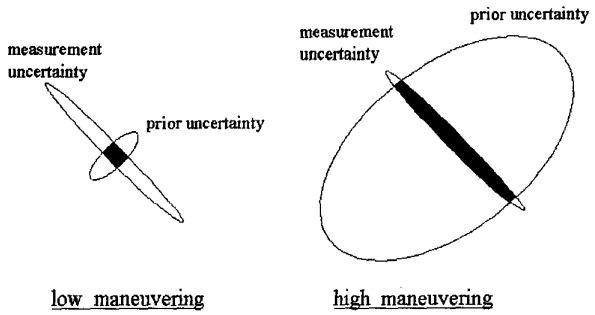

Fig. 11. Heuristics of combination of prior (tracking) and posterior (measurement) information. On left, prior information is of high quality (small σ_v), and hence there is considerably greater sensitivity to orientation of measurement uncertainty as compared to right (large σ_v).

measurements. This is valuable when the velocity varies slowly (low λ_{man}); if the velocity varies rapidly (high λ_{man}), then the enhanced accuracy in velocity measurement of a low sweep rate is more appropriate. Note that the "optimal" sweep rate appears to be in the range of 100 GHz per second: with $N_p = 10$ pulses each of 1 μs duration and coherent processing, this implies a total effective frequency sweep of 1 MHz. It is interesting that this is identical to the "nominal" bandwidth of a 1 μs pulse, and that it appears to be counter-productive to use a larger frequency sweep rate.

2) *Use of an Amplitude Window*: In [6] it was observed that Hamming and/or Gaussian shading (i.e., windowing) of the transmitted pulse [7] had a beneficial effect on tracking in the single-pulse sonar situation, due to the more manageable sidelobe behavior. For the former:

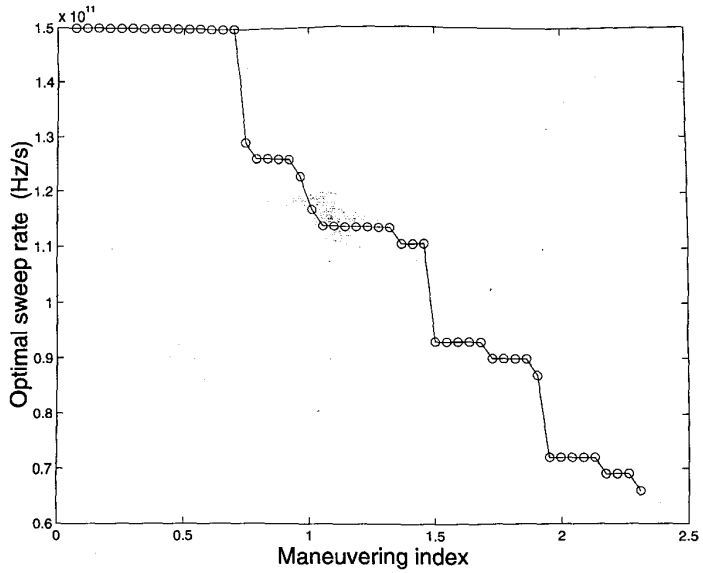

Fig. 12. Optimal LFM sweep rates for $N_p = 10$, $t_p = 1$ μs, $T_R = 5$ μs, plotted as function of maneuvering index. Note that 100 GHz/s sweep rate corresponds to total frequency excursion of 1 MHz.

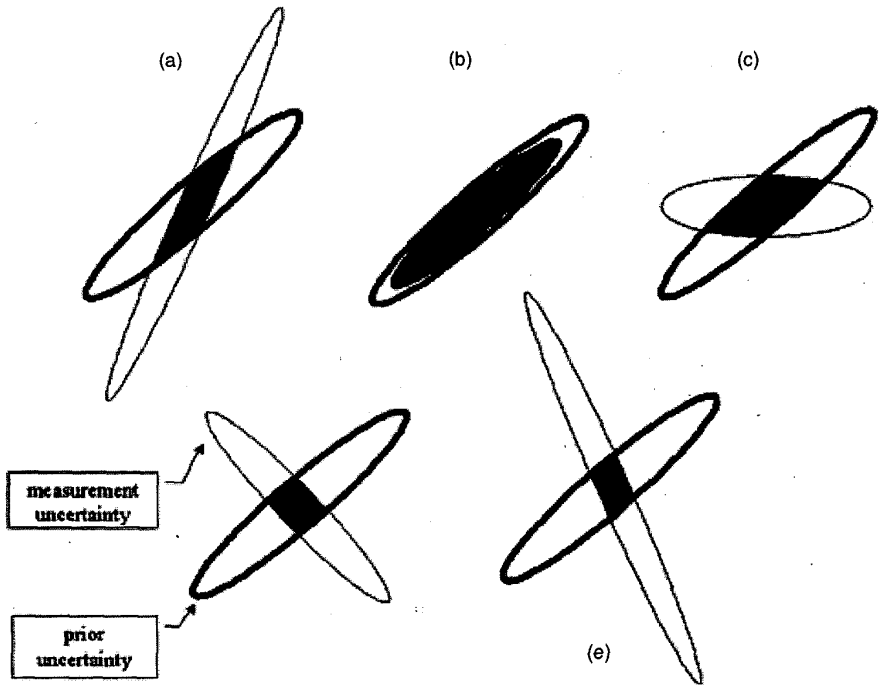

Fig. 13. Explanation of effect of different sweep rates on tracking performance. (a) High negative sweep rate, hence tracking performance as illustrated by intersection between prior and measurement correlation ellipses, is good. (b) Negative sweep rate is such that orientation between prior and measurement ellipses is same—the worst LFM waveform to use. (c) CF situation. (d) Positive LFM sweep, best LFM waveform. (e) LFM upsweep rate is too high, a little enlargement of posterior uncertainty over (d).

$$s_n(t) = \begin{cases} \left[0.08 + 0.92\cos^2 \dfrac{\pi\left(t - \dfrac{t_p}{2}\right)}{t_p}\right] e^{jbt^2} & 0 \le t < t_p \\ 0 & \text{else} \end{cases} \quad (27)$$

Fig. 14 corresponds to the earlier Fig. 9. The situation is less clear in this radar-parameterized situation than for sonar, and indeed it appears that the rectangular shading is somewhat preferable. This may be due to the increased sampling effort ($\alpha = 0.17$) in use here.

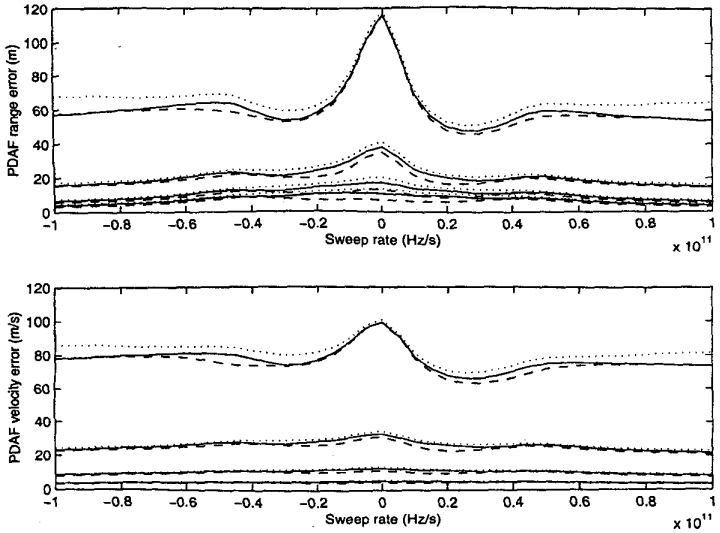

Fig. 14. Estimation range and range-rate error as functions of sweep rate for Hamming-shaded LFM pulse train, $\alpha = 0.17$, $N_p = 20$, $t_p = 10$ μs, $T_R = 50$ μs. In each figure, bottom, middle, and top curves refer to $\sigma_v^2 = 10$, 100, 1,000, and 10,000, corresponding to maneuvering indices $\lambda_{\text{man}} = 0.0073$, 0.023, 0.073, 0.23, respectively. Measurement extraction schemes are strongest return (dotted), direct-average (solid), amplitude-weighted (dashed).

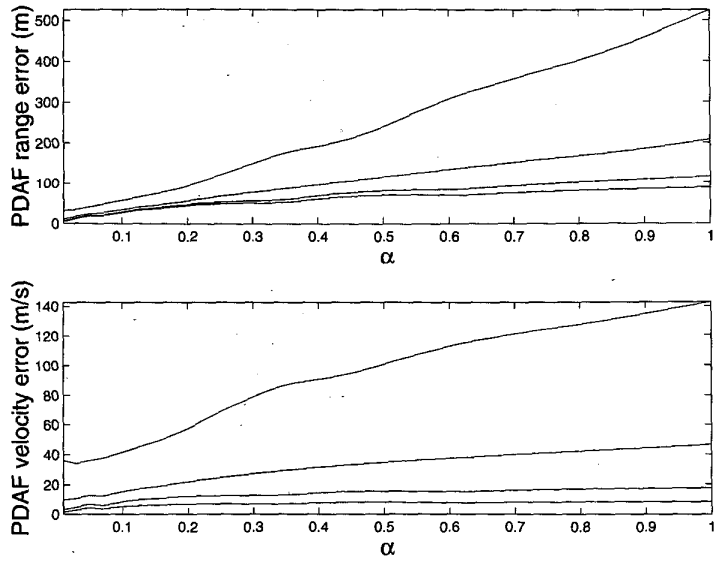

Fig. 15. Estimation range and range-rate error as functions of α (lower α means denser sampling of matched-filter outputs) for rectangular-shaded CF pulse train, $N_p = 20$. In each figure, bottom, middle, and top curves refer to $\sigma_v^2 = 10$, 100, 1,000, and 10,000, corresponding to maneuvering indices $\lambda_{\text{man}} = 0.0073$, 0.023, 0.073, 0.23, respectively. Measurement extraction is by direct-average.

3) *Matched-Filter Sampling Effort*: As mentioned before, the factor α controls the volume of the resolution cell; that is, the sampling in time and Doppler can be scaled by a factor $\sqrt{\alpha}$, with a smaller value of α denoting finer sampling. The results are shown in Fig. 15. From this figure, it is apparent that better performance is available when the sampling is finer. This is not surprising, considering that both measurement accuracy (bounded below by the CRLB on the continuous return $r(t)$ in (3)) and probability of detection (fewer misses from smaller resolution cells) are enhanced by a finer sampling. Naturally, there is cost in terms of computation: the number of matched filters that must be calculated is increased by the factor $1/\alpha$, and the effort devoted to measurement extraction (e.g. centroiding) is increased. From Fig. 15 a compromise value $\alpha = 0.17$ is chosen and is used in subsequent plots.

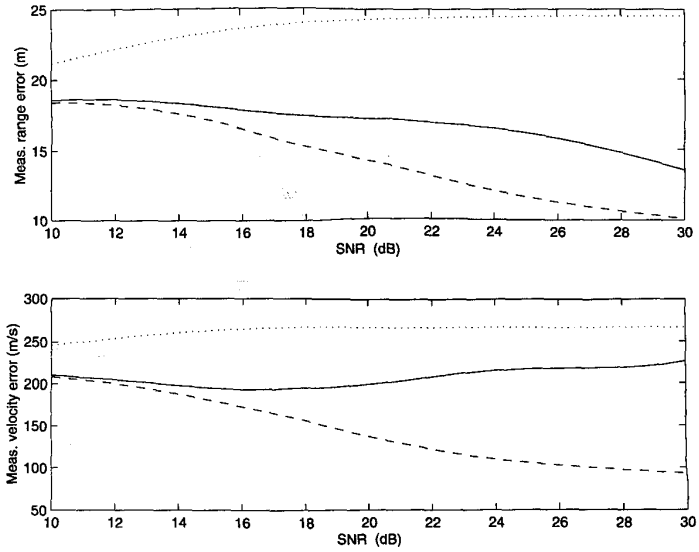

Fig. 16. Measurement range and range-rate error as functions of SNR for Hamming-shaded LFM pulse train, $\alpha = 0.17$, $N_p = 20$, $t_p = 1$ μs, $T_R = 5$ μs. Measurement extraction schemes are strongest return (dotted), direct-average (solid), amplitude-weighted (dashed).

B. Measurement Extraction

1) *Kinds of Measurement Extraction*: Assumption 2 earlier stipulated that when a number of near or contiguous resolution cells yield "hits," then the measurement supplied to the tracker is taken as their average, either direct according to (8) or amplitude-weighted according to (9). We are aware that this is perhaps oversimplified, in that some morphological or image-processing techniques may be used. The procedures appear to be in many cases proprietary and unavailable for general comment. This section presents a simple alternative to these "averaging" schemes, to which they can be compared. The idea is that (8) or (9) is replaced by

$$(\hat{r}(\gamma,r_a,v_a),\hat{v}(\gamma,r_a,v_a)) = \text{argmax}_{(r_g,v_g)}\{\mathcal{A}(\tau_g-\tau_a,f_a-f_g) \quad \text{such that} \quad \gamma\mathcal{A}(\tau_g-\tau_a,f_a-f_g)\geq\eta\} \tag{28}$$

and this may be thought of as a "strongest neighbor" approach, although the correspondence is not exact.

In Figs. 7–9 and 14 the performances of these three measurement extraction schemes are compared versus sweep rate for an LFM pulse. That the strongest neighbor approach of (28) is markedly inferior is clear; there is also some tendency for the amplitude-weighted approach of (9) to be better than the direct-average scheme of (8); this is particularly apparent as regards the measurement accuracy (Fig. 7) but less so when comparing the accuracy of the final estimation (Figs. 9 and 14). The reason for this becomes clear from examination of Figs. 16–18, in which performance is compared against SNR. For low SNRs the averaging schemes are similar. However, as the SNR increases, the small sidelobe "pop-ups" which begin to appear have as much effect in the direct-averaging as do the larger returns; the amplitude-weighting avoids this, and preserves the negative correlation as well.

2) *Avoidance of Measurement Extraction*: An alternative is simply to ignore the issue of measurement extraction, and to communicate *all* threshold exceedances to a PDAF [2]. Since there is no clustering involved here, we call this a *direct-delivery* or *point-measurement* system.[5] On an intuitive level this scheme is appealing, both in its simplicity and in the fact that the PDAF operation will indeed form a weighted sum of the threshold exceedances as its "combined" measurement. The distinction is illustrated in Fig. 19.

The new (direct delivery) scheme is not suitable for evaluation via HYCA, hence our comparisons are on the basis of simulation alone. Simulations are on the basis of 1000 trials of 100 scans each, and initialization is such that the first scan has no measurement uncertainty. The results are shown in Figs. 20–21. Figs. 20 and 21 are also of in-track percentage and of estimation root mean square error (RMSE) for those tracks which are not lost; here the target process noise is held low and the SNR is varied. These results, overall, are somewhat surprising. There appears to be very little difference in terms of track-loss by allowing the PDAF to do the "measurement extraction" itself versus a signal-processing approach in which measurement

[5]The PDAF has implicit to its development the assumption that each target can generate at most one return per scan, hence this last scheme appears to be a deliberate misuse of the tracker.

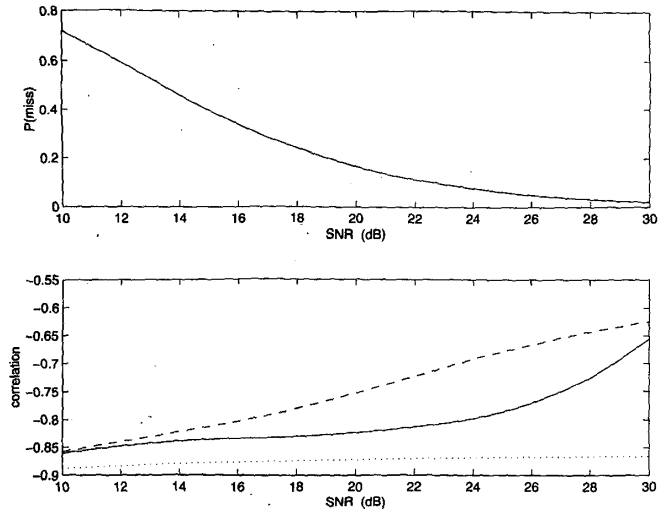

Fig. 17. Probability of miss and range/range-rate correlation coefficient as functions of SNR for Hamming-shaded LFM pulse train, $\alpha = 0.17$, $N_p = 20$, $t_p = 1$ μs, $T_R = 5$ μs. Measurement extraction schemes are strongest return (dotted), direct-average (solid), amplitude-weighted (dashed).

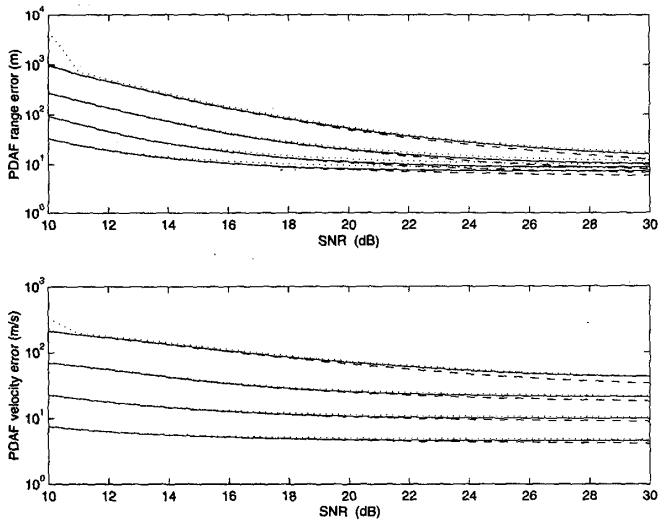

Fig. 18. Estimation range and range-rate error as functions of SNR for Hamming-shaded LFM pulse train, $\alpha = 0.17$, $N_p = 20$, $t_p = 1$ μs, $T_R = 5$ μs. In each figure, bottom, middle, and top curves refer to $\sigma_v^2 = 10$, 100, 1,000, 10,000, corresponding to maneuvering indices $\lambda_{\text{man}} = 0.073$, 0.23, 0.73, 2.3, respectively. Measurement extraction schemes are strongest return (dotted), direct-average (solid), amplitude-weighted (dashed).

extraction is separate from tracking. In terms of estimation error the story is somewhat different, but again the direct-delivery scheme performs well. It appears that the PDAF is quite robust in terms of its assumptions; note that other trackers based on multiple hypothesis tracking (MHT) [4] and assignment do not have the ability to extract a *single* measurement from many, and some sort of measurement-extraction is vital if such a tracker is to be used.

C. Corroboration

1) *Corroboration of Performance Prediction Using HYCA*: Since the HYCA analysis tool is used here, and has indeed been used extensively in our past work to predict performance, a check of its accuracy is perhaps overdue. In fact, there is comparison to simulation in [2, 20, 21]; but since the application here is different, we offer a comparison of HYCA results to simulation.

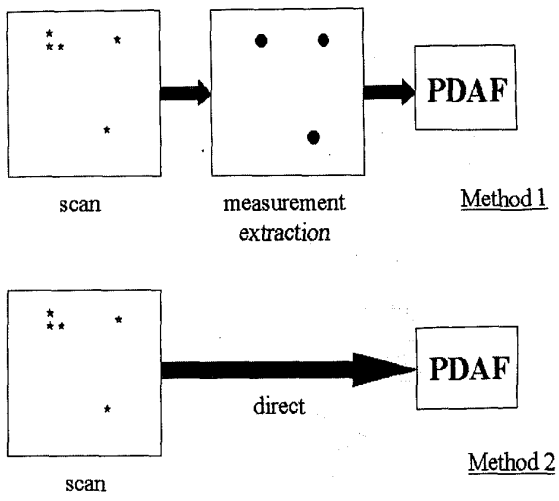

Fig. 19. Method 1 is measurement extraction scheme used here. Measurement delivered to PDAF is direct average of contiguous threshold exceedances. Method 2 is competing method in which *all* measurements are without processing or discrimination delivered directly to PDAF.

In Fig. 22 we show the mean square error (MSE) in range via simulation and using HYCA as a function of scan number for a low-maneuvering target and a CF waveform. The measurement model is as discussed above, and initialization in both cases is without measurement uncertainty (the first measurement is detected and $m_1 = 1$). The correspondence between numerical and analytic results is remarkably good. The HYCA tool appears to be reliable.

2) *Variable Measurement Accuracy*: As originally designed, HYCA takes as input a measurement of accuracy related to measurement covariance matrix $\mathbf{R}$ and probability of detection P_d; both of these are assumed constant, as fits with the standard detection scenario. In our prior analysis we have used the mean measurement accuracy and expected probability of miss according to (10) and (13), respectively, as input; these too are fixed quantities.

It might be argued that this is inappropriate given the assumed measurement-extraction signal processing given in (8) or (9) and shown in Fig. 2. Now, if there is only one threshold exceedance in (8) or (9) then the measurement accuracy may be assumed relatively poor, with covariance equivalent to that of a random variable distributed uniformly within the resolution cell; conversely when there are several (contiguous) threshold exceedances, the accuracy is considerably better due to averaging. The key is that the accuracy is *known to the detector*: the measurement extracted may be considered made up both of location and of an associated accuracy $\mathbf{R}(m_t)$, in which m_t is the number of threshold exceedances (the number of adjacent cells with detections) used in (8) or (9).

This sort of estimation uses measurements of *variable accuracy*, as opposed to the fixed-accuracy situation that each measurement supplied is of the same quality. The original HYCA routine is inappropriate for performance prediction here since it relies on an assumption (actually the PDAF assumption) that each validated measurement is a priori equally likely to be target originated. Thus, to check the effect of the measurement variability we resort to the simplified HYCA of [26] in which, although measurements can be missed, there is no measurement origin uncertainty. The HYCA "state"

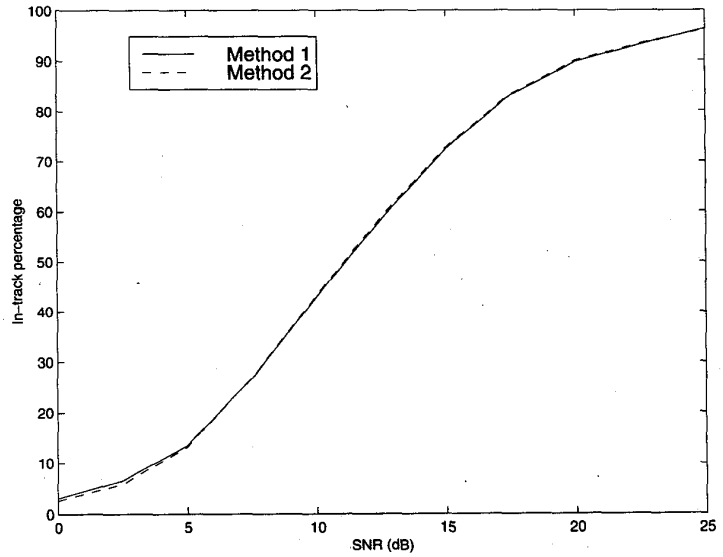

Fig. 20. In-track percentage comparison by simulation of methods 1 (our measurement extraction scheme) and 2 (direct delivery of measurements to PDAF). Waveform is Hamming-weighted LFM pulse with sweep rate 2×10^8 Hz/s, and target process noise has $\sigma_v^2 = 10$.

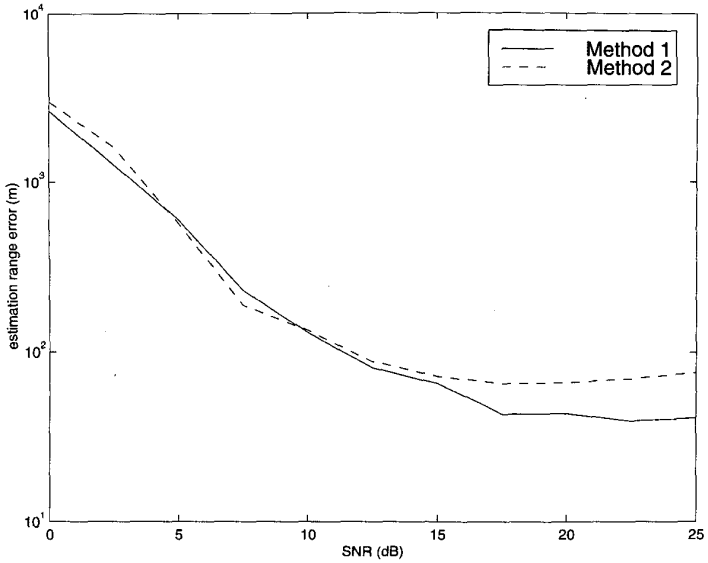

Fig. 21. For those tracks which are not lost, RMSE comparison by simulation of methods 1 (our measurement extraction scheme) and 2 (direct delivery of measurements to PDAF) (see Fig. 20).

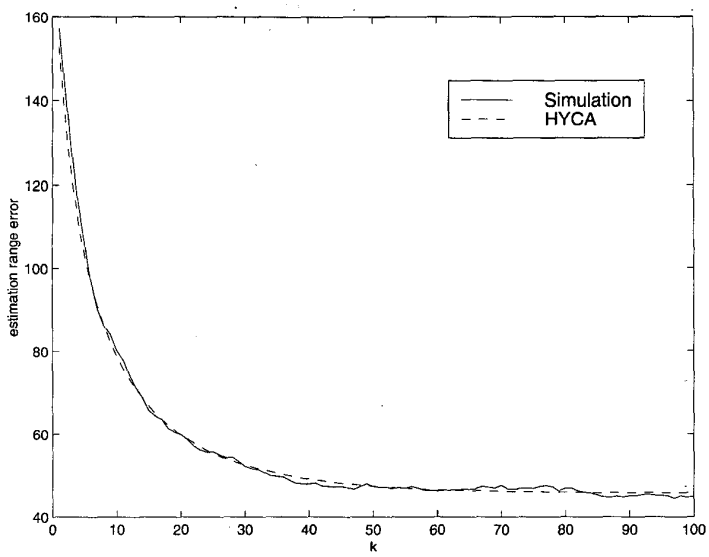

Fig. 22. Comparison of simulation to HYCA's performance prediction in terms of range MSE. Situation is of CF waveform, $\sigma_v^2 = 10$, SNR = 20 dB.

is the number of contiguous threshold exceedances which are averaged for the measurement.

Results are shown in Fig. 23. There is essentially no difference between the variable- and fixed-accuracy situations, and the curves overlie one another. We thus conclude that there is no need to consider measurement accuracy variability.

D. The SDF Receiver

As indicated earlier, the measurement extraction scheme is hampered by the discrete sampling in range and range-rate. That is, a target whose location is not centered within the resolution cell, and is hence not at the respective ambiguity function peak, has a comparatively low probability of detection and may be missed.

This has long been a concern in image detection systems, in which the goal is to detect an object which may have been subjected to a distortion such as rotation or scaling. There have been a number of approaches used, but one of particular success is the "synthetic discriminant function" (SDF) [14]. The SDF idea is to take as a filter the *average* of the filters matched to possible distortions; there is some loss relative to the original matched filter when the object

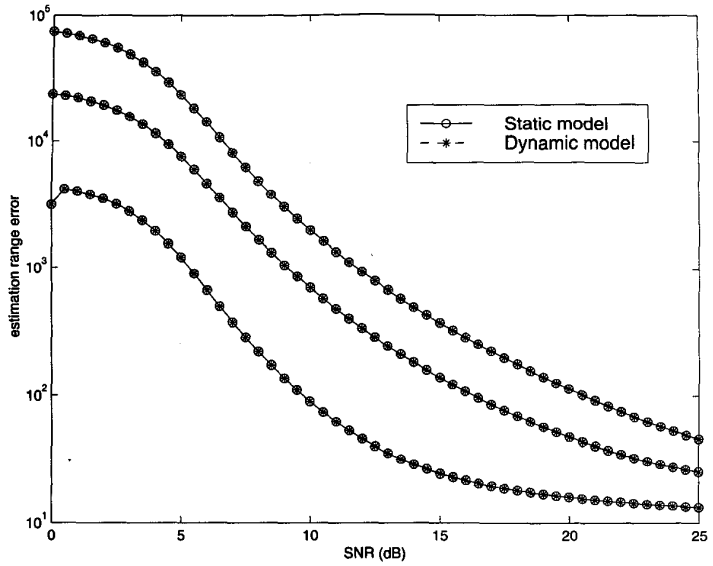

Fig. 23. Range MSE comparison of *static* and *dynamic* measurements via simplified HYCA with no measurement uncertainty. Waveform is Hamming-weighted LFM of sweep rate 20 Hz/s; lower, middle, and top curves have process noise governed by $\sigma_v^2 = 3.33 \times 10^{-6}$, 3.33×10^{-4}, 3.33×10^{-3}, respectively. Parameters here are more appropriate to sonar, but message is clear: results for the two schemes are indistinguishable.

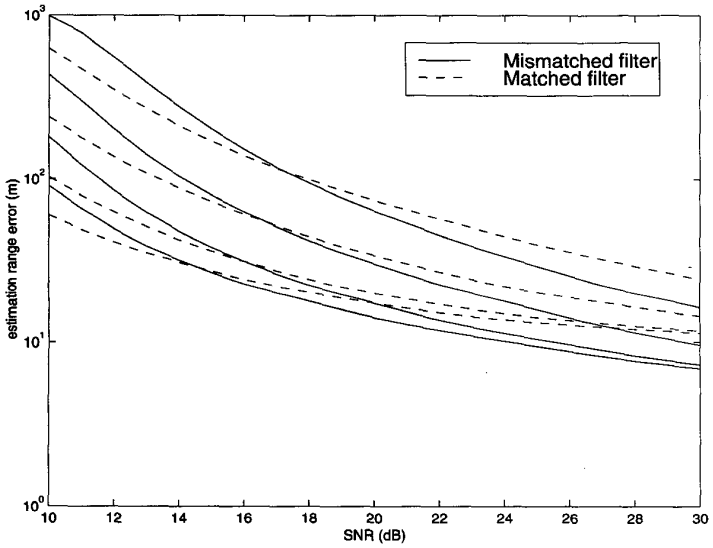

Fig. 24. Range MSE comparison of SDF (mismatched) filter performance to matched filter, for Hamming-weighted LFM waveform with sweep rate 2×10^8 Hz/s, plotted as function of SNR. Lower, middle, and top curves have process noise governed by $\sigma_v^2 = 10$, 100, 1000, and 10,000, respectively.

is undistorted, but the performance over the range of possible objects is robust.

We thus apply the technique here. Note that its application to radar signal processing is similar to the *mismatched* filter [19], except that the goal there is the reduction of ambiguity function sidelobes. With an SDF filter output we have

$$x(\tau_m, f_m) = \int s_{\text{sdf}}^*(\lambda - \tau_m) e^{-j2\pi f_m(\lambda - \tau_m)} r(\lambda) d\lambda \tag{29}$$

replacing (4), in which with respect to (3) we have

$$s_{\text{sdf}}(t) = \int_{(\zeta) \in \mathcal{R}} s(t - 2r/c) e^{j2\pi[-2f_0 v/c]t} dr\, dv \tag{30}$$

as the SDF itself. That is, the SDF is the matched filter *averaged* over all target locations and Doppler shifts possible within the resolution cell $\mathcal{R}$.

Fig. 24, in which the SNR is varied, shows that the SDF is much better than the standard matched filter at high SNRs, but the situation is reversed

when the return strength is poor. We speculate this to be due to the increased tendency for the SDF to produce several contiguous threshold exceedances, and concomitant good measurement accuracy, at high SNR; while at low SNR the reduced detection probability in the resolution cell center yields poorer performance. It would appear that this topic deserves further exploration.

IV. SUMMARY

We have investigated the impact of waveform selection and measurement extraction on radar system (i.e., tracking) performance in the case that both range and range-rate observations are available. Here are the major conclusions.

1) Because of the positive correlation between track estimation errors in position and velocity, tracking is best served by a measurement whose position and velocity errors are negatively correlated. This is easily achieved by LFM upsweep; but the "busy" nature of the ambiguity functions of many fancier waveforms (e.g. VFM, XFM, parabolic FM, and coded CF) destroys this correlation, and their effectiveness in tracking is unimpressive [6, 24]. Further, although an alternating CF/LFM waveform suite performs well, it is seldom as useful as a consistent LFM choice.

2) For each target kinematic model, as expressed by its maneuvering index, there exists a tracking-optimal LFM upsweep frequency rate. This frequency sweep rate increases as the target motion model becomes closer to constant velocity (lower maneuvering index).

3) It is important to control ambiguity function sidelobes. There can be as much as a factor of two improvement when Hamming weighting is used, as compared with the rectangular-envelope case. Hamming weighting appears to be a good choice, in general.

4) The probability of detection for a target not precisely at the point of sampling (i.e., not at the center of a resolution cell) is degraded. Thus, it is worth considering the use of an SDF mismatched filter, which is robust to such perturbations. Results indicate that the performance is SNR dependent: at high SNR it offers a distinct improvement, while at low return strength the ordinary matched filter is better.

5) We have in past work used a measurement extraction system by which contiguous threshold-exceedances (in neighboring resolution cells) are combined to a single measurement, presumably of enhanced accuracy. We have compared this to a *strongest neighbor* approach, and to an amplitude-weighted average; the direct average is a significant improvement over the strongest neighbor scheme. The amplitude-weighted is essentially identical in performance to the direct-average procedure for low-observable targets, but there is a marked improvement in the use of the more-involved amplitude-weighted approach as the SNR grows larger than 20 dB.

6) A simple alternative to these measurement-extraction approaches is direct use of the data association algorithm, basically to give the PDAF target tracker all threshold exceedances and to allow it to extract a combined measurement. Our results show that there is very little loss from the use of this approach. We consider this surprising as the PDAF is designed predicated on an assumption of at most one measurement per target. We note that most alternative tracking algorithms (MHT and assignment) do not immediately allow for "soft" association of multiple returns, and hence in these cases some form of measurement extraction is necessary.

Finally, we note that a popular scheme involves the use of both upsweep and downsweep LFM waveforms—from (1) it is clear that by simple averaging the effect of the target's range-rate can be cancelled. This is the VFM discussed in [6], and when both range and range-rate measurements are available VFM does not perform as well as a consistent use of LFM upsweep. In fact, we conclude that correlated range and range-rate measurements are desirable and should not be avoided.

REFERENCES

[1] Bar-Shalom, Y., Li, X., and Kirubarajau, T. (2001)
Estimation with Application to Tracking Navigation.
Wiley, 2001.

[2] Bar-Shalom, Y., and Li, X. (1995)
Multisensor, Multitarget Tracking: Principles and Techniques.
Storrs, CT: YBS Publishing, 1995.

[3] Bellagarda, J., and Titlebaum, E. (1991)
The hit array: An analysis formalism for multiple access frequency hop coding.
IEEE Transactions on Aerospace and Electronic Systems, **27** (Jan. 1991), 30–39.

[4] Blackman, S., and Popoli, R. (1999)
Design and Analysis of Modern Tracking Systems.
Boston: Artech House, 1999.

[5] Brookner, E. (1998)
Tracking and Kalman Filtering Made Easy.
New York: Wiley, 1998.

[6] Cao, W., Willett, P., Bar-Shalom, Y., and Niu, R. (1998)
Waveform selection based on detection-tracking performance.
In *Proceedings of the SPIE Conference on Signal and Data Processing of Small Targets*, Orlando FL, Apr. 1998.

[7] Cook, C., and Bernfeld, M. (1993)
Radar Signals: An Introduction to Theory and Application.
Dedham, MA: Artech House, 1993.

[8] Costas, R. (1984)
A study of a class of waveforms having nearly ideal range-Doppler ambiguity properties.
Proceedings of the IEEE, Aug. 1984, 996–1009.

[9] Daum, F. (1992)
A system approach to multiple target tracking.
In Y. Bar-Shalom (Ed.), *Multitarget-Multisensor Tracking: Applications and Advances*, vol. II.
Dedham, MA: Artech House, 1992, 149–181.

[10] Fitzgerald, R. (1974)
Effects of range-Doppler coupling on chirp radar tracking accuracy.
IEEE Transactions on Aerospace and Electronic Systems, **AES-10** (July 1974), 528–532.

[11] Fielding, J. (1999)
Polytime coding as a means of pulse compression.
IEEE Transactions on Aerospace and Electronic Systems, **35** (Apr. 1999), 716–721.

[12] Fortmann, T., Bar-Shalom, Y., Scheffé, M., and Gelfand, S. (1985)
Detection thresholds for tracking in clutter—A connection between estimation and signal processing.
IEEE Transactions on Automatic Control (Mar. 1985), 221–228.

[13] Golomb, S., and Taylor, H. (1982)
Two-dimensional synchronization patterns for minimum ambiguity.
IEEE Transactions on Information Theory, **IT-28** (July 1982), 600–604.

[14] Hester, C., and Casasent, D. (1980)
Multivariant technique for multiclass pattern recognition.
Applied Optics, **19** (1980), 1758–1761.

[15] Hong, S., and Evans, R. (2000)
Control of waveforms and detection thresholds for optimal target tracking in clutter.
In *Proceedings of the Conference on Decision and Control* (Dec. 2000), to be published.

[16] Kershaw, D., and Evans, R. (1994)
Optimal waveform selection for tracking systems.
IEEE Transactions on Information Theory (Sept. 1994), 1536–1550.

[17] Kershaw, D., and Evans, R. (1997)
Waveform selective probabilistic data association.
IEEE Transaction on Aerospace and Electronic Systems, **33** (Oct. 1997), 1180–1188.

[18] Levanon, N. (1988)
Radar Principles.
New York: Wiley, 1988.

[19] Lewis, B., Kretschner, B., and Shelton, W. (1996)
Aspects of Radar Signal Processing.
Boston: Artech House, 1996.

[20] Li, X., and Bar-Shalom, Y. (1994)
Stability evaluation and track life of the PDAF for tracking in clutter.
IEEE Transactions on Automatic Control (May 1991), 588–602.

[21] Li, X., and Bar-Shalom, Y. (1994)
Detection threshold selection for tracking performance optimization.
IEEE Transactions on Aerospace and Electronic Systems, **29** (July 1994), 742–749.

[22] Maric, S., and Titlebaum, E. (1990)
Frequency hop multiple access codes based upon the theory of cubic congruences.
IEEE Transactions on Aerospace and Electronic Systems, **26** (Nov. 1990), 1035–1039.

[23] Niu, R., Willett, P., and Bar-Shalom, Y. (1999)
System-level performance of radar waveforms.
In *Proceedings of the 1999 Mediterranean Conference on Control and Automation*, Haifa, Israel, June 1999.

[24] Niu, R., Willett, P., and Bar-Shalom, Y. (1999)
From the waveform through the resolution cell to the tracker.
In *Proceedings of the 1999 Aerospace Conference*, Snowmass, CO, Mar. 1999.

[25] Willett, P., Niu, R., and Bar-Shalom, Y. (2000)
Waveform detection tracking performance at the system level.
In Y. Bar-Shalom and W. Blair (Eds.), *Multitarget-Multisensor Tracking: Applications and Advances*.
Boston: Artech House, 2000.

[26] Rago, C., Willett, P., and Bar-Shalom, Y. (1998)
Detection-tracking performance with combined FM-CW waveforms.
IEEE Transactions on Aerospace and Electronic Systems, **34** (Apr. 1998), 612–624.

[27] Scheer, I., and Kurtz, J. (1993)
Coherent Radar Performance Estimation.
Norwood, MA: Artech House, 1993.

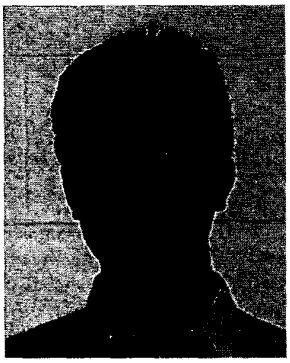

Ruixin Niu received his B.S. degree from Xi'an Jiaotong University, Xi'an, China, in 1994, his M.S. degree from Institute of Electronics, Chinese Academy of Sciences, Beijing, in 1997, and his Ph.D. degree from the University of Connecticut, Storrs, in 2001, all in electrical engineering.

He is currently a postdoctoral researcher at Syracuse University, Syracuse, NY working in the signal processing area. His research interests lie in signal/image processing, detection, and estimation theory.

Peter Willett (S'83—M'86) received the B.A.Sc. in 1982 from the University of Toronto, Toronto, Canada, and the Ph.D. from Princeton University, Princeton, NJ, in 1986.

He is a Professor at the University of Connecticut, Storrs, where he has worked since 1986. His interests are generally in the areas of detection theory and signal processing, and, lately, particularly in the area of data fusion.

Yaakov Bar-Shalom (S'63—M'66—SM'80—F'84) was born on May 11, 1941. He received the B.S. and M.S. degrees from the Technion, Israel Institute of Technology, in 1963 and 1967 and the Ph.D. degree from Princeton University, Princeton, NJ, in 1970, all in electrical engineering.

From 1970 to 1976 he was with Systems Control, Inc., Palo Alto, CA. Currently he is School of Engineering Distinguished Professor in the Dept. of Electrical and Computer Engineering and Director of the ESP Lab (Estimation and Signal Processing) at the University of Connecticut. His research interests are in estimation theory and stochastic adaptive control and he has published over 270 papers in these areas. In view of the causality principle between the given name of a person (in this case, "(he) will track", in the modern version of the original language of the Bible) and the profession of this person, his interests have focused on tracking.

He coauthored the monograph *Tracking and Data Association* (Academic Press, 1988), the graduate texts *Estimation and Tracking: Principles, Techniques and Software* (Artech House, 1993), *Multitarget-Multisensor Tracking: Principles and Techniques* (YBS Publishing, 1995), *Estimation with Applications to Tracking and Navigation* (Wiley 2001), and edited the books *Multitarget-Multisensor Tracking: Applications and Advances* (Artech House, Vol. I 1990; Vol. II 1992; Vol. III 2000). He has been elected Fellow of IEEE for "contributions to the theory of stochastic systems and of multitarget tracking." He has been consulting to numerous companies, and originated the series of Multitarget-Multisensor Tracking short courses offered via UCLA Extension, at Government Laboratories, private companies, and overseas. He has also developed the commercially available interactive software packages MULTIDAT TM for automatic track formation and tracking of maneuvering or splitting targets in clutter, PASSDAT TM for data association from multiple passive sensors, BEARDAT TM for target localization from bearing and frequency measurements in clutter, IMDAT TM for image segmentation and target centroid tracking and FUSEDAT TM for fusion of possibly heterogeneous multisensor data for tracking. During 1976 and 1977 he served as Associate Editor of the *IEEE Transactions on Automatic Control* and from 1978 to 1981 as Associate Editor of the *IEEE Transactions on Automatic Control* and from 1978 to 1981 as Associate Editor of *Automatica*. He was Program Chairman of the 1982 American Control Conference, General Chairman of the 1985 ACC, and Co-Chairman of the 1989 IEEE International Conference on Control and Applications. During 1983–1987 he served as Chairman of the Conference Activities Board of the IEEE Control Systems Society and during 1987–1989 was a member of the Board of Governors of the IEEE CSS. Currently he is a member of the Board of Directors of the International Society of Information Fusion and served as ISIF President in 2000 and 2002. In 1987 he received the IEEE CSS Distinguished Member Award. Since 1995 he is a Distinguished Lecturer of the IEEE AESS. He is co-recipient of the M. Barry Carlton Award for the best paper in the *IEEE Transactions on Aerospace and Electronic Systems* in 1995, and received the 1998 University of Connecticut AAUP Excellence Award for Research.